# Pd and Pt complexes of Benzo-Fused Dipyrrins. Synthesis, Structure, Electrochemical and Optical Properties

Graden Snyder,<sup>1</sup> Sara Abuhadba,<sup>1</sup> Neo Lin,<sup>2</sup> Wei-Tsung Lee,\*,<sup>3</sup> Tomoyasu Mani,\*,<sup>2</sup> and Tatiana V. Esipova\*,<sup>1</sup>

- <sup>1</sup> Department of Chemistry and Biochemistry, Loyola University Chicago, Chicago, IL 60660, USA.
- <sup>2</sup> Department of Chemistry, University of Connecticut, Storrs, CT 06269-3060, USA.
- <sup>3</sup> Department of Chemistry, National Central University, Taoyuan 32001, Taiwan.

KEYWORDS: dipyrrin, benzo-fused dipyrrin, metal complexes of dipyrrins.

**ABSTRACT:** Benzo-fused dipyrrins are  $\pi$ -extended analogs of conventional dipyrrins, which exhibit bathochromically shifted absorption and possess the synthetic capability to bind various metal ions. We aimed to investigate the synthetic potential of benzo-fused dipyrrins in complexation with transition metals. Two new complexes with  $Pd^{2+}$  and  $Pt^{2+}$  were synthesized, and characterized. X-ray crystallography reveals that both complexes exhibited a zigzag geometry with square planar coordination of the central metal. The  $Pd^{2+}$  complex possesses a very weak fluorescence at 665 nm while the  $Pt^{2+}$  complex is completely nonemissive. Transient absorption spectroscopy confirmed triplet excited state formation for both complexes, however they are short-lived and no phosphorescence was observed even at 77K. DFT calculations support the experimental observation, revealing the existence of the low-lying ligand-metal charge-transfer (LMCT) triplet state, acting as an energy sink.

#### INTRODUCTION

Dipyrrins, frequently described as "half porphyrins", represent a fascinating class of organic chromophores. Owing to their rich and diverse coordination chemistry, they form complexes with a variety of metal ions. The most popular and stable complex of dipyrrin with boron difluoride, known as BODIPY, is widely used as a fluorophore for biomedical applications, such as imaging,<sup>1-6</sup> sensing,<sup>7-13</sup> and photodynamic therapy.<sup>14-21</sup> On the other hand, dipyrrin complexes with transition metals can be advantageous for catalysis,<sup>22,23</sup> the preparation of coordination polymers,<sup>24-26</sup> metal-organic frameworks<sup>27-35</sup> and self-assembly of supramolecules,<sup>36-38</sup> due to the facile complexation reactions.

Benzo-fused dipyrrins, in which each of two conjugated pyrrole units is fused with the benzene ring, possess a bathochromic shift in absorption spectra due to extended  $\pi$ -conjugation and therefore can be particularly interesting for biomedical<sup>21, 39, 40</sup> and material science applications, such as solar cell technology,<sup>41, 42</sup> circularly polarized luminescence materials, 43 and Optical Power Limiting (OPL) filters. 44 However, in contrast to regular dipyrrins, there is limited information available regarding complexes of benzo-fused dipyrrins with transition metals. Only a singular report exists describing complexation with Zn2+, Ca2+, and some lanthanide ions, with isolation and characterization of solely Zn<sup>2+</sup> complex.<sup>45</sup> Herein, we present a facile room-temperature procedure for the preparation of homoleptic palladium and platinum complexes of benzo-fused dipyrrins and discuss their electrochemical and optical properties.

## Scheme 1. Synthesis of benzodipyrrin complexes $Pd(L)_2$ and $Pt(L)_2$ .

$$\begin{array}{c} \text{BuO}_2\text{C} \\ \text{CHO} \\ \text{CO}_2\text{Et} \\ \text{BuO}_2\text{C} \\ \text{CO}_2\text{Bu} \\ \text{EtO}_2\text{C} \\ \text{(L)H. } 82\% \\ \text{CO}_2\text{Et} \\ \text{iii or iv} \\ \\ \text{BuO}_2\text{C} \\ \text{OEt} \\ \text{EtO} \\ \text{CO}_2\text{Bu} \\ \text{M= Pd, Pt} \\ \text{CO}_2\text{Bu} \\ \text{M= Pd, Pt} \\ \text{Pd(L)2. } 82\% \\ \text{Pt(L)2. } 75\% \\ \end{array}$$

Reaction conditions: (i): CH<sub>2</sub>Cl<sub>2</sub>, TFA, r.t., 24 h; (ii): CH<sub>2</sub>Cl<sub>2</sub>, DDQ, r.t., 2 h; (iii): 1) K<sub>2</sub>CO<sub>3</sub>, THF, r.t., 24 h, 2) PdCl<sub>2</sub>(COD), THF, r.t., 48 h; (iv): 1) K<sub>2</sub>CO<sub>3</sub>, THF, r.t., 24 h, 2) PtCl<sub>2</sub>(COD), THF, r.t., 72 h.

#### RESULTS AND DISCUSSION

**Synthesis.** The benzo-fused dipyrrin ((**L)H**), which we used for the preparation of  $Pd^{2+}$  and  $Pt^{2+}$  complexes, is shown in **Scheme 1**. Diethoxycarbonyl substituents in the

alpha positions of benzo-fused dipyrrin, and 3,5-dibutoxycarbonyl substituents in the meso-phenyl ring should render it soluble in organic solvents. Benzo-fused dipyrrin (L)H was prepared with an 82% yield from 4,7-dihydroisoindole and an aldehyde using an oxidative aromatization approach<sup>45</sup> (**Scheme 1**). For the preparation of the palladium complex of benzo-fused dipyrrin **Pd(L)**<sub>2</sub>, we initially attempted a procedure developed for the complexation of regular dipyrrins. 46-48 This procedure involves treating the ligand with a Pd2+ salt, usually in the presence of a base, such as triethylamine. However, these methods were unsuccessful in our case. We hypothesized that, firstly, ethoxyearbonyl substituents in the alpha positions of benzodipyrrin units might create steric hindrance that prevents homoleptic complexation. Secondly, compared to regular dipyrrin, binding of the benzodipyrrin units to Pd2+ might be weaker due to the reduced nucleophilicity of the chelating nitrogen atoms, arising from a combination of increased  $\pi$ -delocalization into the benzene rings and electron-withdrawing character of alpha-ethoxycarbonyl groups. To gain more insights into the reaction, we decided to split it into two steps: the deprotonation of benzodipyrrin (L)H with a base of alkali metal, followed by the transmetalation with a Pd<sup>2+</sup> salt. We speculated that alkali bases should efficiently deprotonate the nitrogen atom of benzodipyrrin due to stabilization of the formed anion by the electron withdrawing alpha-ethoxycarbonyls on the one hand, and the benzofused rings on the other. The deprotonation of the benzodipyrrin (L)H with an excess of K<sub>2</sub>CO<sub>3</sub> proceeded smoothly in a tetrahydrofuran solution at room temperature. While the reaction proceeded, we observed the reaction mixture gradually changing color from deep purple to deep blue. In the second step, we attempted transmetalation with Pd<sup>2+</sup> to

form the desired Pd(L)<sub>2</sub> from the benzodipyrrin alkali metal complex. Though various Pd2+ salts were used, including PdCl<sub>2</sub>, Pd(OAc)<sub>2</sub>, and PdCl<sub>2</sub>(COD), only the reaction with PdCl<sub>2</sub>(COD) led to the formation of the palladium complex Pd(L)<sub>2</sub> after stirring in a tetrahydrofuran solution for 48 hours at room temperature. The color of the reaction mixture gradually changed from deep blue to teal. The Pd(L)<sub>2</sub> complex was isolated with 82% yield by crystallization from a benzene/pentane mixture. As mentioned above, initially, we were concerned about the successful binding of (L)H to Pd<sup>2+</sup> and the overall stability of Pd(L)<sub>2</sub> complex due to the steric bulk of (L)H and the reduced nucleophilicity of chelating nitrogen atoms. Surprisingly, the palladium complex of benzodipyrrin Pd(L)2 proved to be stable and could be easily purified using column chromatography on silica gel. Interestingly, when we used a stronger base - lithium diisopropylamide- to deprotonate benzodipyrrin in the first step, a mixture of products was formed, which was hard to separate and identify. Increasing the temperature in the second step did not significantly affect the reaction, and the highest yields were obtained when the reaction proceeded at room temperature.

Inspired by this result, we opted to prepare a platinum analogue  $Pt(L)_2$  by treating potassium benzodipyrrin with  $Pt^{2+}$  salts. Similarly, among the various platinum salts used, including  $PtCl_2$ ,  $Pt(acac)_2$  and  $PtCl_2(COD)$ , only the reaction with  $PtCl_2(COD)$  resulted in the formation of desired platinum complex of benzodipyrrin  $Pt(L)_2$  after 72 hours of stirring in a tetrahydrofuran solution at room temperature. The  $Pt(L)_2$  complex was isolated with 75% yield by crystallization from diethyl ether. Similar to the  $Pd(L)_2$  complex, it showed good stability during column chromatography on silica gel.

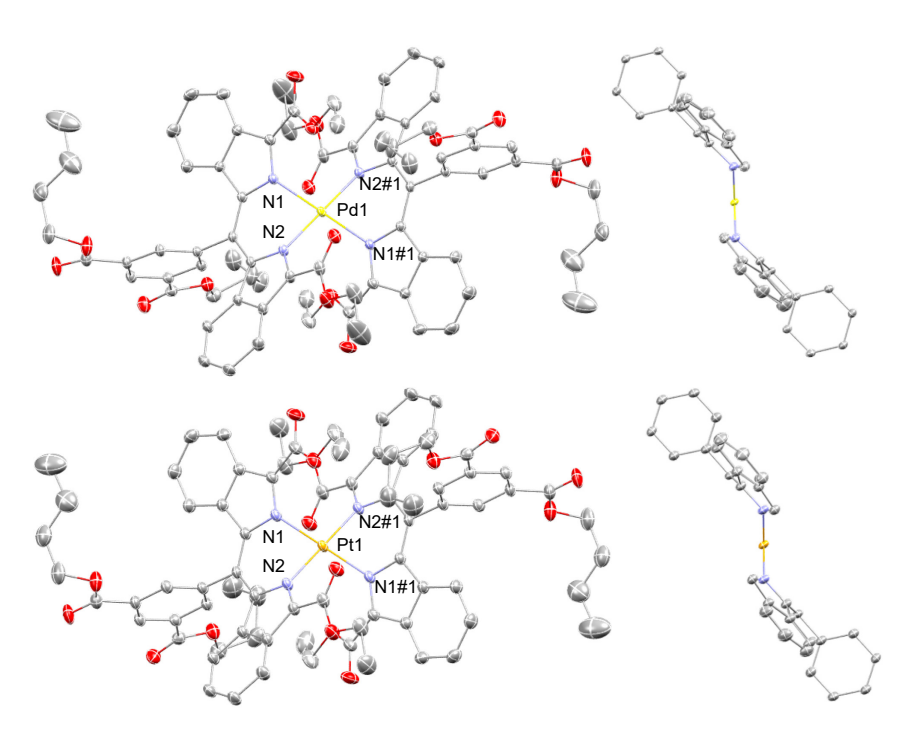


Figure 1. Left: molecular structures of benzodipyrrin complexes  $Pd(L)_2$  (top) and  $Pt(L)_2$  (bottom) with thermal ellipsoids at the 50% probability level. Hydrogen atoms and solvent molecules are omitted for clarity. Right: side views of  $Pd(L)_2$  (top) and  $Pt(L)_2$  complexes with truncated ester groups. Color key: yellow = Pd, orange = Pt, blue = N, grey = C, red = O

The  $Pd(L)_2$  and  $Pt(L)_2$  complexes exhibit remarkable solubility in both polar and nonpolar solvents, including N,N-dimethyl formamide, tetrahydrofuran, acetonitrile, 1,4-dioxan, diethyl ether, dichloromethane, toluene and benzene. This versatility enhances their potential usability across various applications.

**Solid-state structure.** Single crystals of  $Pd(L)_2$  and  $Pt(L)_2$  complexes suitable for X-ray diffraction analysis were obtained by slow diffusion of n-pentane into a benzene solution and from a concentrated diethyl ether solution at ambient temperature, respectively. Detailed crystallographic data are presented in **Table 1**, and the molecular structures of  $Pd(L)_2$  and  $Pt(L)_2$  complexes are depicted in **Figure 1**, S1 and S2.

Both complexes,  $Pd(L)_2$  and  $Pt(L)_2$ , exhibit intriguing similarities in their solid-state characteristics. They are isostructural, crystallizing in the triclinic space group  $P\overline{1}$ . Both complexes are four coordinate, adopt a square planar environment ( $\tau_4 = 0$  for both compounds), and the Pd<sup>2+</sup> and Pt<sup>2+</sup> centers lie perfectly in the coordination planes constituted by four nitrogen atoms (out of plane distance = 0 Å). In addition, due to the bulky coordination sphere, the interligand bite angles ∠N1#1-M-N2 are relatively larger than that of intraligand ones, ∠N1-M-N2. Some interesting structural features arise from the difference in ionic radius of each metal. For example, the larger ionic radius of Pd2+ results in longer Pd-N bonds (average  $d_{Pd-N}$ = 2.011 Å) in comparison to Pt-N bonds (average  $d_{Pd-N}$ = 2.005 Å). Consequently, the smaller intraligand bite angles ∠N1-M-N2 observed for  $Pd(L)_2$  complex (85.16(4)°) comparing to those of in  $Pt(L)_2$  complex (94.84(4)°).

Interestingly, instead of planar geometry, the benzodipyrrin ligands are bent to reduce steric repulsion, and tilted to MN<sub>4</sub> plane, resulting in a zigzag configuration (**Figure 1** right). However, when comparing to a structural analogue, bis-dipyrrinato-Pd(II)<sup>48</sup>, the dihedral angle of the two pyrrole planes found in benzodipyrrin complexes  $Pd(L)_2$  (156.67°) and  $Pt(L)_2$  (151.65°) are less bent although they have greater steric bulkiness. In both complexes benzodipyrrin ligands are tilted by 135.9° ( $Pd(L)_2$ ) and 138.3° ( $Pt(L)_2$ ) to the MN<sub>4</sub> planes.

**Table 1.** Selected bond distances (Å), angles (°), and dihedral angles (°) for  $Pd(L)_2$  and  $Pt(L)_2$  complexes.<sup>a</sup>

Pd <sup>2+</sup> -complex		Pt <sup>2+</sup> -complex	
Pd1-N1	2.0156(10)	Pt1-N1	2.0004(15)
Pd1-N2	2.0057(10)	Pt1-N2	2.0105(16)
	,		
N1-Pd1-N2	85.16(4)	N1-Pt1-N2	82.29(6)
N1#1-Pd1-N2	94.84(4)	N1#1-Pt1-N2	93.71
N1-Pd1-N1#1	180.0	N1-Pt1-N1#1	180.0
N2-Pd1-N2#1	180.0	N2-Pt1-N2#1	180.0
C8-C9-C10-C11	164.16(13)	C8-C9-C10-C11	162.48(18)
C9-C10-C24-C29	86.43(15)	C9-C10-C22-C23	82.9(2)
τ4	0	τ4	0

<sup>&</sup>lt;sup>a</sup> Numbers in parentheses are standard uncertainties in the last significant figures. Atoms are labeled as indicated in Figures 1, S1 and S2. Symmetry operations: #1 = -x+1, -y+1, -z+1

The *meso*-phenyl substituents in benzodipyrrin ligands maintain nearly perpendicular orientations with respect to benzodipyrrin planes, forming angles of approximately 86.4° and 82.9° in **Pd(L)**<sub>2</sub> and **Pt(L)**<sub>2</sub> complexes, respectively.

Remarkably, in both  $Pd(L)_2$  and  $Pt(L)_2$  complexes, the alpha-ethoxycarbonyl substituents extend in the benzodipyrrin planes, forming a sandwich-like structure and thereby not interfering with complexation.

**Electrochemical properties.** The reduction potentials of  $Pd(L)_2$  and  $Pt(L)_2$  complexes of benzodipyrrins were determined using cyclic voltammetry (CV) and differential pulse voltammetry (DPV). The voltammograms are shown in Figure S3-8, and the reduction potentials are reported in **Table 2**.

**Table 2.** Electrochemical properties of  $Pd(L)_2$  and  $Pt(L)_2$  complexes<sup>a</sup>

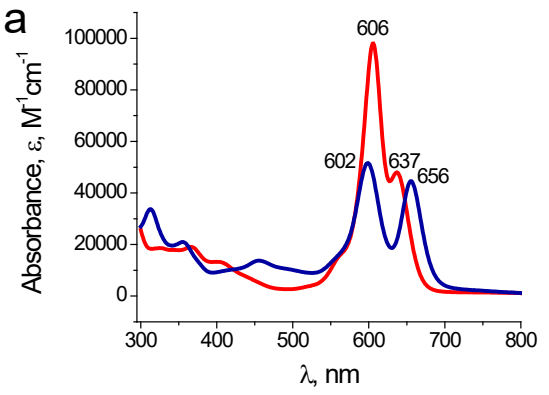
	$E_{ox}$	$E_{red}$	$E_{red}^2$
Pd(L) <sub>2</sub>	$0.41^{\rm b}$	-1.02	-1.44
$Pt(L)_2$	$0.34^{\rm b}$	-1.11	-1.50

<sup>a</sup> Reported V vs.  $Fc^{+/0}$ . Measured in acetonitrile with 0.1 M TBA+PF<sub>6</sub>-. The errors are usually 10-20 mV. <sup>b</sup> Irreversible.

For both  $Pd(L)_2$  and  $Pt(L)_2$  complexes, voltammograms exhibit two reversible waves corresponding to the reduction potentials of the neutral form  $(E_{red})$  and the radical anion  $(E_{red}^2)$ . We report reduction potentials vs Fc<sup>+/0</sup>. The reduction potentials for the Pd(L)2 complex are -1.02 and -1.44 V, while for the Pt(L)2 complex, they are -1.11 and -1.50 V. These values are closely matched, which is not surprising since both complexes share isoelectronic and isostructural nature. The slight differences in the potentials might be attributed to the influence of distinct metal ions involved.  $E_{\rm red}$  values are  $\sim 0.2$  V more negative than that of the benzo-fused BODIPY with alpha-ethoxycarbonyl substituents (-0.84 V) but  $\sim$ 0.4-0.5 V more positive than that of the benzo-fused BODIPY with methyl substituents (-1.53 V).49 This difference also suggests that central metals affect the reduction potentials ( $E_{red}$ ) in these molecules, which is further supported by our TDDFT calculations (see below).

In the positive region of voltammograms, we detected broad irreversible waves for both complexes, corresponding to the reduction of radical cations ( $E_{ox}$ ). The reduction potential for the Pd(L)<sub>2</sub> complex is approximately 0.41 V, while for the **Pt(L)**<sup>2</sup> complex, it is 0.34 V. These values are significantly lower than the reported reduction potential (0.82 V) for the radical cation of benzo-fused BODIPY with ethoxycarbonyl substituents in alpha-positions. Instead, they more closely resemble the reduction potential (0.33 V) observed for the radical cation of benzo-fused BODIPY with alpha-methyl substituents.49 We hypothesized that alphaethoxycarbonyl substituents might be decoupled from the  $\pi$ -electronic system of benzodipyrrin ligands in the solutions of Pd(L)<sub>2</sub> and Pt(L)<sub>2</sub> complexes. Therefore, their electron-withdrawing effect is much lower than that of benzofused BODIPY molecules. Our TDDFT calculations suggest that metals do not cause a sufficient effect on the reduction potential of radical cations ( $E_{ox}$ ) in these molecules.

**Optical spectroscopy.** The absorption and emission spectra of the  $Pd(L)_2$  complex and the absorption spectrum of the  $Pt(L)_2$  complex are shown in **Figure 2**, and the



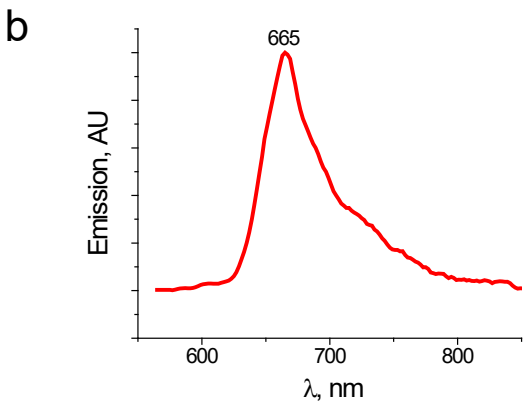


Figure 2. (a) Absorption spectra of  $Pd(L)_2$  (red) and  $Pt(L)_2$  (dark blue) complexes in acetonitrile; (b) Emission spectrum of  $Pd(L)_2$  complex in toluene at r.t.

selected photophysical parameters are summarized in **Table 3**. We observed the two main absorption bands around 600 nm for both  $Pd(L)_2$  and  $Pt(L)_2$  complexes. For the  $Pd(L)_2$  complex, we detect an intense band centered at  $\lambda_{max} = 606$  nm, which is accompanied by a secondary peak at  $\lambda = 637$  nm, exhibiting an intensity approximately half of the primary peak. In the case of the  $Pt(L)_2$  complex, the second absorption band is more pronounced. Thereby we observe a band at  $\lambda_{max} = 602$  nm. This band exhibits a lower intensity compared to the  $Pd(L)_2$  complex ( $\varepsilon$  is about a half of the  $Pd(L)_2$  complex), and it is accompanied by another band at  $\lambda = 656$  nm, which possess almost equivalent intensity. We will discuss the origin of these bands in the later section (TDDFT calculations).

**Table 3.** Photophysical characteristics of  $Pd(L)_2$  and  $Pt(L)_2$  complexes.

$ au^{ m b}$ $ au^{ m b}$
(ns)
.0038 0.8b/0.72a
A NA

<sup>&</sup>lt;sup>a</sup> Reported in acetonitrile. <sup>b</sup> Reported in toluene.

In both cases, these intense absorption bands are significantly red-shifted relative to the  $Pd^{2+}$  complex of regular dipyrrin ( $\lambda_{max} = 476$  nm),<sup>48</sup> but are close to the reported benzo-fused BODIPY molecules.<sup>43,49</sup>

We observed very weak room-temperature fluorescence for  $Pd(L)_2$  complex in acetonitrile and toluene, with  $\lambda_{max}=665$  nm. In toluene solution, the quantum yield for this fluorescence was measured to be  $\Phi_{\rm fl}=0.0038$  and fluorescence lifetime  $\tau_{\rm fl}=0.8$  ns. In contrast, the  $Pt(L)_2$  complex showed no observable emission. Interestingly, neither of these complexes possesses any phosphorescence, even at a low temperature of 77K in frozen toluene. We performed both femtosecond (fsTA) and nanosecond (nsTA) transient absorption spectroscopy to elucidate photophysical characteristics further.

Transient Absorption Spectroscopy. fsTA data of the Pd(L)<sub>2</sub> and Pt(L)<sub>2</sub> complexes in acetonitrile are shown in Figure 3. We analyzed the fsTA data by a global fit to produce evolution-associated difference spectra (EADS) in a sequential model<sup>50</sup> or decay-associated spectra (DAS). The data of the Pd(L)2 complex revealed a very fast decay of the initially formed excited states ( $\tau_1$  = 300 fs), followed by the formation of another short-lived species ( $\tau_2 = 9$  ps), and then by a relatively long-lived component that is already decaying within the time window (~8 ns) of our fsTA instrument  $(\tau_3 = 4 \text{ ns})$ . The spectral shape of this long-lived component is consistent with the species captured by nsTA, revealing a lifetime of only  $\sim 10$  ns (**Figure 3a, b**). Note that the nsTA measurements were conducted in deoxygenated solutions to avoid possible quenching by molecular oxygens. The data of the Pt(L)<sub>2</sub> complex also revealed a fast decay of the initial excited state ( $\tau_1 = 1.5 \text{ ps}$ ) and two other species ( $\tau_2 = 100 \text{ ps}$ and  $\tau_3$  =1.2 ns). The spectral shape of the longer-lived component is consistent with the species captured by nsTA, revealing a lifetime of only ~6 ns (**Figure 3c**). One interesting feature of the Pt(L)2 complex data is the bleaching and recovery of the peak at ~450 nm, which corresponds to the appearance and decay of the longer-lived species (Figure 3d). The observation indicates that this band has characteristics different from the initial excited states (see Photophysical Pathway section).

We observed a similar photodynamic behavior in a significantly more nonpolar solvent - benzene. EADS of the **Pd(L)**<sub>2</sub> complex in benzene are shown in Figure S9.

**Computations.** We performed DFT calculations to gain further insights into these complexes' excited state dynamics. We optimized the ground states of  $Pd(L)_2$  and  $Pt(L)_2$  complexes with Ci symmetry, which agree well with the X-ray crystal structures. The structures with  $D_2$  symmetry are energetically much higher ( $\sim 1$  eV) than those with the  $C_1$ . The bulkiness of alpha-ethoxycarbonyl groups of benzodipyrrins makes the conformation with  $D_2$  symmetry structurally inaccessible. When optimized without symmetrical constraint, a symmetry-broken structure ( $C_1$ ) is slightly energetically higher than the symmetric one ( $C_1$ ). In contrast, the  $Pd^2$  complex of a regular dipyrrin without alpha substitutions is reported to convert between the two conformations ( $C_1$  and  $D_2$ ).<sup>48</sup>

In the following, we first discuss the absorption features of these complexes. We performed TDDFT calculations in acetonitrile (Table S2 and S3 for  $Pd(L)_2$  and  $Pt(L)_2$ , respectively). TDDFT calculations at the  $C_i$  (and  $C_1$ ) ground state geometry show four major singlet excited states (S1-4

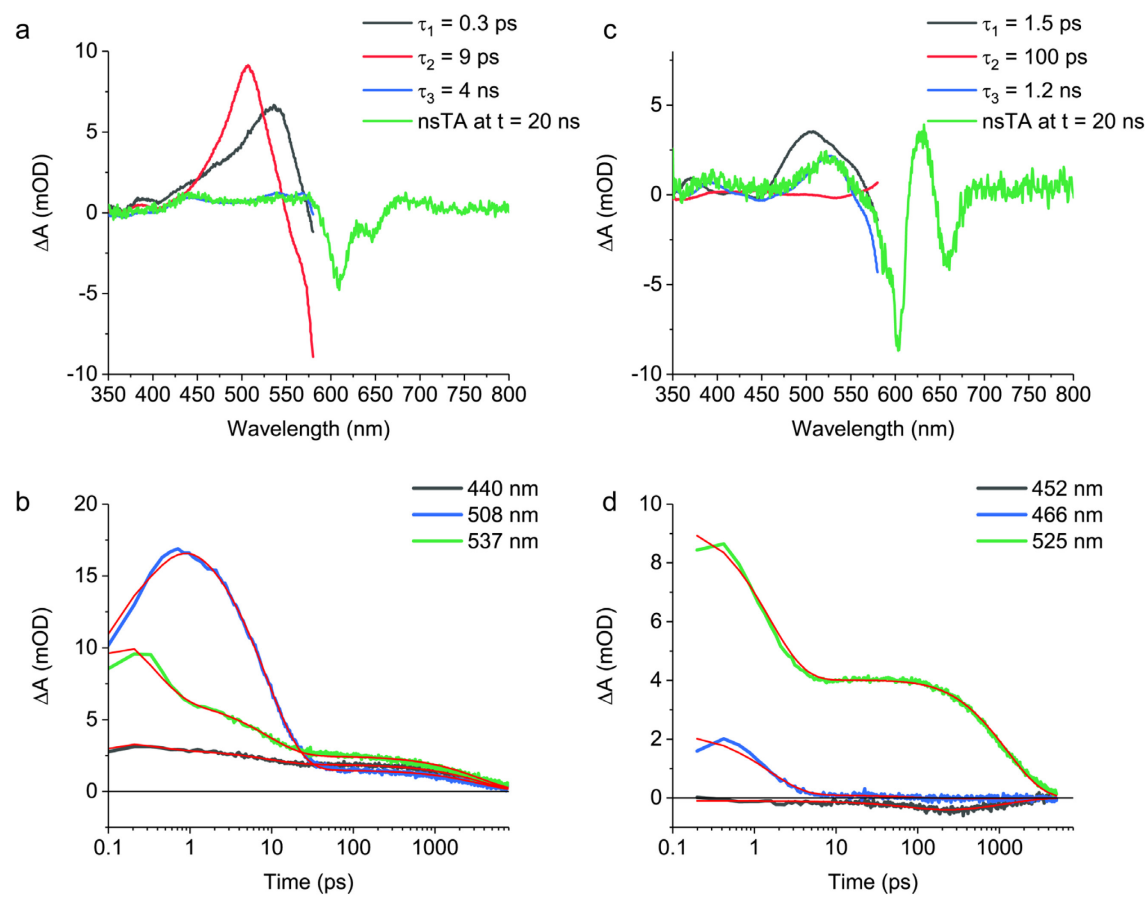


**Figure 3.** (a) EADS of the fsTA data for the  $Pd(L)_2$  complex ( $\lambda_{ex} = 600$  nm), along with the nsTA spectrum at 20 ns after the excitation pulse of  $\lambda_{ex} = 600$  nm. (b) Decay kinetics at 440, 508, and 537 nm for the  $Pd(L)_2$  complex ( $\lambda_{ex} = 600$  nm). The red lines are fitted curves. (c) DAS of the fsTA data for the  $Pt(L)_2$  complex ( $\lambda_{ex} = 630$  nm), along with the nsTA spectrum at 20 ns after the excitation pulse of  $\lambda_{ex} = 630$  nm. (d) Decay kinetics at 452, 466, and 525 nm for the  $Pt(L)_2$  complex ( $\lambda_{ex} = 630$  nm). The red lines are fitted curves. Note that the heights of the nsTA spectra in panel a and b are adjusted.

in **Figure 4**) whose major contributions come from the two HOMOs and two LUMOs. HOMO-1, HOMO, and LUMO+1 are ligand-centered while LUMO has a significant metal contribution (**Figure 4**). Note that this significant metal contribution in LUMO likely contributes to  $E_{\rm red}$  mentioned above. Among the four states, one with a "pure" LC transition (HOMO-1  $\rightarrow$  LUMO+1, S4) and one with a ligand-to-metal charge-transfer (LMCT) transition (HOMO  $\rightarrow$  LUMO, S1 or  $^{1}$ LMCT<sub>1</sub>) are symmetry-forbidden. We call these two states (S1 and S4)  $^{1}$ LMCT<sub>1</sub> and  $^{1}$ LC<sub>2</sub>, respectively.

We identified the two symmetry-allowed transitions (oscillator strength, f > 0) and they are S2 and S3 in **Figure 4**. The transition of largest oscillator strength is higher in energy (S3) and has the mixture of the "pure" LC and LMCT characters with a larger LMCT contribution ( $^1$ LMCT $_2$ ). The transition of lower oscillator strength is lower in energy (S2) and has almost "pure" LC characteristics ( $^1$ LC $_1$ ). We therefore assign the state of higher oscillator strength to the main transition observed experimentally;  $\lambda_{max} = 606$  and 602 nm for the **Pd(L)** $_2$  and **Pt(L)** $_2$  complexes, respectively. This assignment agrees with the reported Pd $_2$ + complex of regular dipyrrin. In addition to these main transitions, we observed another band  $\lambda = 637$  and 656 nm for the **Pd(L)** $_2$  and **Pt(L)** $_2$  complexes (**Figure 2**). The energy differences between the two transitions are  $\Delta E = 800$  cm $_2$ 1 and 1370 cm $_2$ 2.

<sup>1</sup>, respectively. We assigned this lower energy state to <sup>1</sup>LMCT<sub>2</sub> (i.e., S2 in **Figure 4**).

An alternative explanation of these two energy transitions can be exciton coupling<sup>51,52</sup> of the localized LC benzodipyrrin transitions, which are polarized along the long axis of benzodipyrrin ligand. Here, the two transition dipole moments are aligned in parallel, resulting in an enhanced absorbance to the higher-energy excited state (H-type exciton coupling), 53, 54 agreeing with the observations. The energy difference of the two transitions,  $\Delta E$ , corresponds to twice the exciton coupling energy. A similar exciton coupling phenomenon was observed for the analogous complexes of regular dipyrrins with metals.48 However, considering the structural similarity between the Pt(L)2 and Pd(L)2 complexes, we would expect  $\Delta E$  to be about the same for the Pt(L)2 complex. If these bands had arisen from exciton coupling, the observed difference in  $\Delta E$  suggests that the solution-state structures of Pd(L)<sub>2</sub> and Pt(L)<sub>2</sub> are significantly different. Another possible explanation of these two bands is vibronic progression caused by a vibrational mode likely corresponding to C=C stretching in the excited state. If the splitting were due to vibronic progression, we would also expect both complexes to exhibit the same pattern, which is not the case here. While our results cannot fully rule out these alternatives, we currently concluded that the

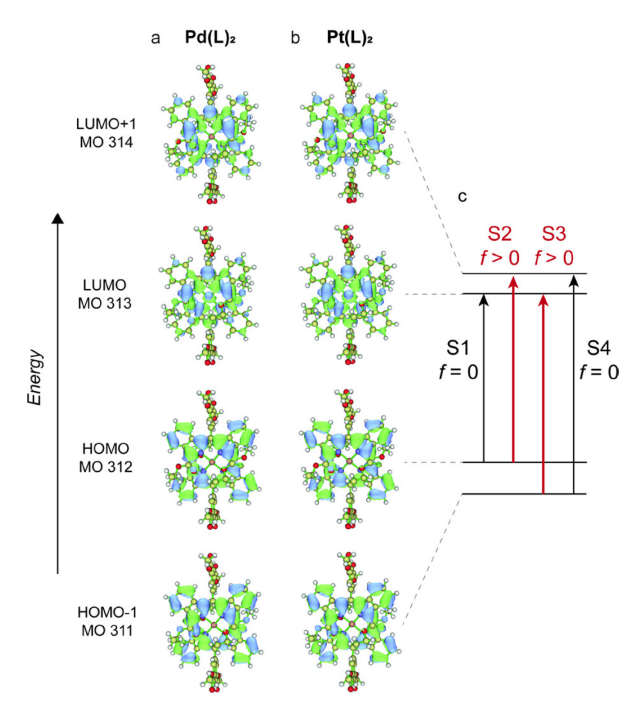


**Figure 4.** Visualization of molecular orbitals for (a) **Pd(L)**2 and (b) **Pt(L)**2 complex. The calculations were performed at the level of PBE1PBE/SDS-6-31G(d). (c) The arrow represents the largest transitions contributing to the first four singlet excited states identified in the TDDFT calculations.

observed two transitions stem from the two different electronic states ( ${}^{1}LC_{1}$  and  ${}^{1}LMCT_{2}$ ).

TDDFT calculations also revealed that the triplet excited states of dominant LC characters ( $^3$ LC states) of these benzodipyrrin complexes are energetically higher than the triplet excited states of dominant  $^3$ LMCT state as a zigzag configuration prevents exciton (electron/hole) delocalization in a plane unlike their counterparts of  $Pd^{2+}$  and  $Pt^{2+}$  tetrabenzoporphyrin where exciton is delocalized in a plane. $^{55,56}$ 

**Photophysical pathway.** With the experimental and computational data in hand, we would like to map out the photophysical pathways. The state diagrams of the **Pd(L)**<sub>2</sub> and **Pt(L)**<sub>2</sub> complexes are shown in **Figure 5**.

For the **Pd(L)**<sup>2</sup> complex, the initial photoexcitation at the main transition band can populate both <sup>1</sup>LMCT and <sup>1</sup>LC<sub>1</sub> states, which decay very quickly via internal conversion to form the spin-allowed LMCT state (1LMCT1). 1LMCT1 then undergoes ISC to form the low-energy triplet excited state (3LMCT). The rate of ISC in the  $Pd(L)_2$  complex (~ 9 ps) is comparable to other Pd<sup>2+</sup> complexes reported.<sup>48, 57, 58</sup> The zigzag geometry of the Pd(L)2 complex may slightly diminish the heavy atom effect of Pd<sup>2+</sup> compared to a planar Pd<sup>2+</sup> tetrabenzoporphyrin. In consistency with the Pd<sup>2+</sup> complex of regular dipyrrin, 48 we assigned the final and lowest energy state as 3LMCT state whose lifetime is only ~10 ns for the Pd(L)2 complex. While we conclude this as the major pathway here, we cannot completely exclude another pathway, namely the formation of 3LC by ISC and then IC to <sup>3</sup>LMCT (dotted lines in **Figure 5a**). <sup>3</sup>LC → <sup>3</sup>LMCT internal conversion could proceed so quickly that the concentration of 3LC might be too small to capture reliably at room temperature. 3LMCT states are known to be nonemissive. 48,59

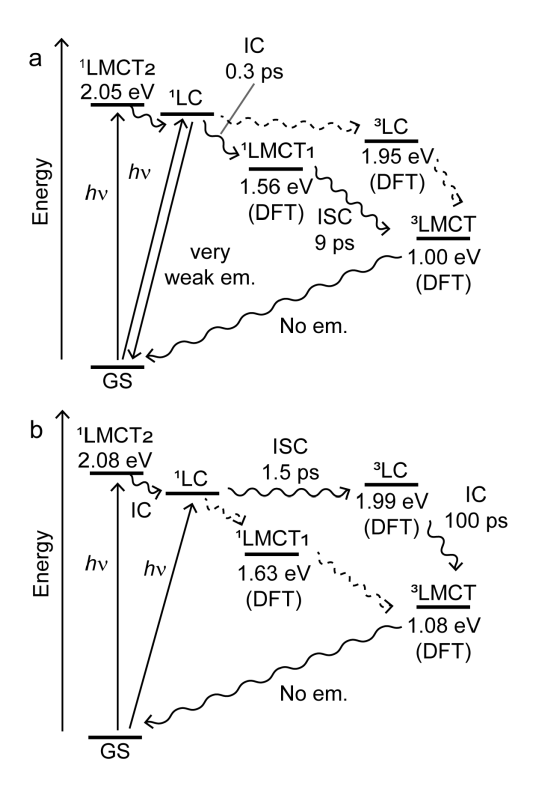


**Figure 5.** State diagrams of (a) **Pd(L)**<sub>2</sub> and (b) **Pt(L)**<sub>2</sub> complexes in acetonitrile. IC = internal conversion; ISC = intersystem crossing.

In a similar manner to the Pd(L)2 complex, we assigned the final nonemissive state of Pt(L)<sub>2</sub> as a <sup>3</sup>LMCT state whose lifetime is ~6 ns. However, the photophysical pathway leading to this final state appears different. Photoexcitation leads to the formation of <sup>1</sup>LMCT<sub>2</sub> and <sup>1</sup>LC<sub>1</sub> states. The fast decay of these initial excited states ( $\tau_1 \sim 1.5$  ps) results in the formation of <sup>3</sup>LC by ISC, which is then followed by a relatively slow internal conversion ( $\tau_2 \sim 100$  ps) to populate <sup>3</sup>LMCT. The bleaching and recovery of the LMCT-centered transition (450 nm in **Figure 3d**) we observed in fsTA support our assignment. The rate of ISC is slightly slower than that of Pt<sup>2+</sup> tetrabenzoporphyrin;  $1/k_{\rm ISC} \sim 0.4$  ps.<sup>60</sup> This slightly slow ISC may again be due to the zigzag conformation of the Pt(L)<sub>2</sub> complex. An alternative pathway is shown in Figure 5b as dotted lines, which is similar to the pathway of **Pd(L)**<sup>2</sup> (IC and ISC to form <sup>3</sup>LMCT<sub>1</sub>).

Unlike the Pd<sup>2+</sup> complex of regular dipyrrin, in which the low-temperature measurements could capture phosphorescence from <sup>3</sup>LC,<sup>48</sup> we did not observe any new emission from benzodipyrrin complexes Pd(L)<sub>2</sub> and Pt(L)<sub>2</sub> at 77K. In both cases, non-emitting and fast-decaying <sup>3</sup>LMCT acts as an energy sink in these compounds, resulting in the almost complete absence of emission.

#### CONCLUSIONS

In conclusion, the synthesis and characterization of two new highly soluble complexes of benzo-fused dipyrrins with Pd²+ and Pt²+ have been achieved, encompassing structural, spectroscopic, and electrochemical analysis. The identified complexes possess robust absorption within the  $\lambda$  = 600 – 700 nm region. The formation of nonemissive triplet excited states was confirmed for both complexes. This research offers insights into the synthetic capabilities of

benzo-fused dipyrrins, paving the way for their application in the field of coordination chemistry and materials science.

#### ASSOCIATED CONTENT

Figure S1-15, Table S1-S3, experimental details, synthetic procedures, and NMR data.

This material is available free of charge via the Internet at http://pubs.acs.org.

#### **AUTHOR INFORMATION**

#### **Corresponding Authors**

\* <u>tesipova@luc.edu</u>, <u>tomoyasu.mani@uconn.edu</u>, <u>wlee5@ncu.edu.tw</u>

#### **Author Contributions**

All authors have given approval to the final version of the manuscript.

#### **ACKNOWLEDGMENT**

The authors acknowledge funding by the National Science Foundation under Grant No. 2247661 (T.E.), 2247662 (T.M.) and by the National Science and Technology Council of Taiwan (Grant NSTC 112–2113-M-008–013). The computational studies were performed at the cluster located in the Chemistry Division of the Brookhaven National Laboratory through work funded by LDRD 23-030 (T.M.). The acquisition of a tunable nanosecond laser system (Opolette UX10230U, Opotek) was supported by the University of Connecticut CLAS Research Equipment Funding.

#### **REFERENCES**

- (1) Sirbu, D.; Luli, S.; Leslie, J.; Oakley, F.; Benniston, A. C. Enhanced in vivo Optical Imaging of the Inflammatory Response to Acute Liver Injury in C57BL/6 Mice Using a Highly Bright Near-Infrared BODIPY Dye. *ChemMedChem* **2019**, *14* (10), 995-999. DOI: <a href="https://doi.org/10.1002/cmdc.201900181">https://doi.org/10.1002/cmdc.201900181</a>.
- (2) Franke, J. M.; Raliski, B. K.; Boggess, S. C.; Natesan, D. V.; Koretsky, E. T.; Zhang, P.; Kulkarni, R. U.; Deal, P. E.; Miller, E. W. BODIPY Fluorophores for Membrane Potential Imaging. *Journal of the American Chemical Society* **2019**, *141* (32), 12824-12831. DOI: 10.1021/jacs.9b05912.
- (3) Gupta, N.; Reja, S. I.; Bhalla, V.; Gupta, M.; Kaur, G.; Kumar, M. A bodipy based dual functional probe for the detection of hydrogen sulfide and H2S induced apoptosis in cellular systems. *Chemical Communications* **2015**, *51* (54), 10875-10878, 10.1039/C5CC02984H. DOI: 10.1039/C5CC02984H.
- (4) Lim, S.; Haque, M. M.; Su, D.; Kim, D.; Lee, J.-S.; Chang, Y.-T.; Kim, Y. K. Development of a BODIPY-based fluorescent probe for imaging pathological tau aggregates in live cells. *Chemical Communications* **2017**, *53* (10), 1607-1610, 10.1039/C6CC08826K. DOI: 10.1039/C6CC08826K.
- (5) Brizet, B.; Goncalves, V.; Bernhard, C.; Harvey, P. D.; Denat, F.; Goze, C. DMAP-BODIPY Alkynes: A Convenient Tool for Labeling Biomolecules for Bimodal PET–Optical Imaging. *Chemistry A European Journal* **2014**, *20* (40), 12933-12944. DOI: https://doi.org/10.1002/chem.201402379.
- (6) Kowada, T.; Maeda, H.; Kikuchi, K. BODIPY-based probes for the fluorescence imaging of biomolecules in living cells. *Chemical Society Reviews* **2015**, *44* (14), 4953-4972, 10.1039/C5CS00030K. DOI: 10.1039/C5CS00030K.
- (7) Niu, L.-Y.; Guan, Y.-S.; Chen, Y.-Z.; Wu, L.-Z.; Tung, C.-H.; Yang, Q.-Z. BODIPY-Based Ratiometric Fluorescent Sensor for Highly

- Selective Detection of Glutathione over Cysteine and Homocysteine. *Journal of the American Chemical Society* **2012**, *134* (46), 18928-18931. DOI: 10.1021/ja309079f.
- (8) Pakhomov, A. A.; Belova, A. S.; Khchoyan, A. G.; Kononevich, Y. N.; Ionov, D. S.; Maksimova, M. A.; Frolova, A. Y.; Alfimov, M. V.; Martynov, V. I.; Muzafarov, A. M. Ratiometric Singlet Oxygen Sensor Based on BODIPY-DPA Dyad. *Molecules* **2022**, *27* (24), 9060.
- (9) Sui, B.; Tang, S.; Liu, T.; Kim, B.; Belfield, K. D. Novel BODIPY-Based Fluorescence Turn-on Sensor for Fe3+ and Its Bioimaging Application in Living Cells. *ACS Applied Materials & Interfaces* **2014**, *6* (21), 18408-18412. DOI: 10.1021/am506262u.
- (10) Vendrell, M.; Krishna, G. G.; Ghosh, K. K.; Zhai, D.; Lee, J.-S.; Zhu, Q.; Yau, Y. H.; Shochat, S. G.; Kim, H.; Chung, J.; et al. Solid-phase synthesis of BODIPY dyes and development of an immunoglobulin fluorescent sensor. *Chemical Communications* **2011**, *47* (29), 8424-8426, 10.1039/C1CC11774B. DOI: 10.1039/C1CC11774B.
- (11) Kuimova, M. K.; Yahioglu, G.; Levitt, J. A.; Suhling, K. Molecular Rotor Measures Viscosity of Live Cells via Fluorescence Lifetime Imaging. *Journal of the American Chemical Society* **2008**, *130* (21), 6672-6673. DOI: 10.1021/ja800570d.
- (12) Vyšniauskas, A.; Cornell, B.; Sherin, P. S.; Maleckaitė, K.; Kubánková, M.; Izquierdo, M. A.; Vu, T. T.; Volkova, Y. A.; Budynina, E. M.; Molteni, C.; et al. Cyclopropyl Substituents Transform the Viscosity-Sensitive BODIPY Molecular Rotor into a Temperature Sensor. *ACS Sensors* **2021**, *6* (6), 2158-2167. DOI: 10.1021/acssensors.0c02275.
- (13) Kolemen, S.; Akkaya, E. U. Reaction-based BODIPY probes for selective bio-imaging. *Coordination Chemistry Reviews* **2018**, *354*, 121-134. DOI: <a href="https://doi.org/10.1016/j.ccr.2017.06.021">https://doi.org/10.1016/j.ccr.2017.06.021</a>.
- (14) Ozdemir, T.; Bila, J. L.; Sozmen, F.; Yildirim, L. T.; Akkaya, E. U. Orthogonal Bodipy Trimers as Photosensitizers for Photodynamic Action. *Organic Letters* **2016**, *18* (19), 4821-4823. DOI: 10.1021/acs.orglett.6b02418.
- (15) Nguyen, V.-N.; Yim, Y.; Kim, S.; Ryu, B.; Swamy, K. M. K.; Kim, G.; Kwon, N.; Kim, C.-Y.; Park, S.; Yoon, J. Molecular Design of Highly Efficient Heavy-Atom-Free Triplet BODIPY Derivatives for Photodynamic Therapy and Bioimaging. *Angewandte Chemie International Edition* **2020**, *59* (23), 8957-8962. DOI: https://doi.org/10.1002/anie.202002843.
- (16) Turksoy, A.; Yildiz, D.; Akkaya, E. U. Photosensitization and controlled photosensitization with BODIPY dyes. *Coordination Chemistry Reviews* **2019**, *379*, 47-64. DOI: https://doi.org/10.1016/j.ccr.2017.09.029.
- (17) Lincoln, R.; Durantini, A. M.; Greene, L. E.; Martínez, S. R.; Knox, R.; Becerra, M. C.; Cosa, G. meso-Acetoxymethyl BODIPY dyes for photodynamic therapy: improved photostability of singlet oxygen photosensitizers. *Photochemical & Photobiological Sciences* **2017**, *16* (2), 178-184. DOI: 10.1039/c6pp00166a.
- (18) Yin, J.; Jiang, X.; Sui, G.; Du, Y.; Xing, E.; Shi, R.; Gu, C.; Wen, X.; Feng, Y.; Shan, Z.; et al. The tumor phototherapeutic application of nanoparticles constructed by the relationship between PTT/PDT efficiency and 2,6- and 3,5-substituted BODIPY derivatives. *Journal of Materials Chemistry B* **2021**, 9 (36), 7461-7471, 10.1039/D1TB01155C. DOI: 10.1039/D1TB01155C.
- (19) Wang, J.; Gong, Q.; Jiao, L.; Hao, E. Research advances in BODIPY-assembled supramolecular photosensitizers for photodynamic therapy. *Coordination Chemistry Reviews* **2023**, 496, 215367. DOI: <a href="https://doi.org/10.1016/j.ccr.2023.215367">https://doi.org/10.1016/j.ccr.2023.215367</a>.
- (20) Mai, D. K.; Kang, B.; Temmy Pegarro, V.; Isabel Wen, B.; Cho, S.; Lee, J.; Kim, E.; Ho-Joong, K. Synthesis and Photophysical Properties of Tumor-Targeted Water-Soluble BODIPY Photosensitizers for Photodynamic Therapy. *Molecules* **2020**, *25* (15), 3340. DOI: <a href="https://doi.org/10.3390/molecules25153340">https://doi.org/10.3390/molecules25153340</a> Publicly Available Content Database.
- (21) Mao, Z.; Kim, J. H.; Lee, J.; Xiong, H.; Zhang, F.; Kim, J. S. Engineering of BODIPY-based theranostics for cancer therapy. *Coordination Chemistry Reviews* **2023**, *476*, 214908. DOI: https://doi.org/10.1016/j.ccr.2022.214908.
- (22) Baek, Y.; Betley, T. A. Catalytic C–H Amination Mediated by Dipyrrin Cobalt Imidos. *Journal of the American Chemical Society* **2019**, *141* (19), 7797-7806. DOI: 10.1021/jacs.9b01262.

- (23) Dong, Y.; Clarke, R. M.; Porter, G. J.; Betley, T. A. Efficient C—H Amination Catalysis Using Nickel-Dipyrrin Complexes. *Journal of the American Chemical Society* **2020**, *142* (25), 10996-11005. DOI: 10.1021/jacs.0c02126.
- (24) Béziau, A.; Baudron, S. A.; Hosseini, M. W. Heterometallic coordination polymers incorporating dipyrrin based heteroleptic copper and cobalt complexes: to Ag– $\pi$  or not? *Dalton Transactions* **2012**, *41* (24), 7227-7234, 10.1039/C2DT30549F. DOI: 10.1039/C2DT30549F.
- (25) Moutier, F.; Khalil, A. M.; Baudron, S. A.; Lescop, C. Gleaned snapshots on the road to coordination polymers: heterometallic architectures based on Cu(i) metallaclips and 2,2′-bis-dipyrrin metalloligands. *Chemical Communications* **2020**, *56* (72), 10501-10504, 10.1039/D0CC04862C. DOI: 10.1039/D0CC04862C.
- (26) Béziau, A.; Baudron, S. A.; Rasoloarison, D.; Hosseini, M. W. Rigid yet flexible heteroleptic Co(iii) dipyrrin complexes for the construction of heterometallic 1- and 2-D coordination polymers. *CrystEngComm* **2014**, *16* (23), 4973-4980, 10.1039/C4CE00273C. DOI: 10.1039/C4CE00273C.
- (27) Béziau, A.; Baudron, S. A.; Fluck, A.; Hosseini, M. W. From Sequential to One-Pot Synthesis of Dipyrrin Based Grid-Type Mixed Metal-Organic Frameworks. *Inorganic Chemistry* **2013**, *52* (24), 14439-14448. DOI: 10.1021/ic402892f.
- (28) Baudron, S. A. Luminescent metal—organic frameworks based on dipyrromethene metal complexes and BODIPYs. *CrystEngComm* **2016**, *18* (25), 4671-4680, 10.1039/C6CE00450D. DOI: 10.1039/C6CE00450D.
- (29) Halper, S. R.; Cohen, S. M. Heterometallic Metal—Organic Frameworks Based on Tris(dipyrrinato) Coordination Complexes. *Inorganic Chemistry* **2005**, *44* (3), 486-488. DOI: 10.1021/ic048289z.
- (30) Murphy, D. L.; Malachowski, M. R.; Campana, C. F.; Cohen, S. M. A chiral, heterometallic metal-organic framework derived from a tris(chelate) coordination complex. *Chemical Communications* **2005**, (44), 5506-5508, 10.1039/B510915A. DOI: 10.1039/B510915A.
- (31) Halper, S. R.; Do, L.; Stork, J. R.; Cohen, S. M. Topological Control in Heterometallic Metal–Organic Frameworks by Anion Templating and Metalloligand Design. *Journal of the American Chemical Society* **2006**, *128* (47), 15255-15268. DOI: 10.1021/ja0645483.
- (32) Garibay, S. J.; Stork, J. R.; Wang, Z.; Cohen, S. M.; Telfer, S. G. Enantiopure vs. racemic metalloligands: impact on metal—organic framework structure and synthesis. *Chemical Communications* **2007**, (46), 4881-4883, 10.1039/B712118K. DOI: 10.1039/B712118K.
- (33) Stork, J. R.; Thoi, V. S.; Cohen, S. M. Rare Examples of Transition-Metal—Main-Group Metal Heterometallic Metal—Organic Frameworks from Gallium and Indium Dipyrrinato Complexes and Silver Salts: Synthesis and Framework Variability. *Inorganic Chemistry* **2007**, *46* (26), 11213-11223. DOI: 10.1021/ic7016159.
- (34) Béziau, A.; Baudron, S. A.; Pogozhev, D.; Fluck, A.; Hosseini, M. W. Stepwise construction of grid-type Cu(ii)-Cd(ii) heterometallic MOFs based on an imidazole-appended dipyrrin ligand. *Chemical Communications* **2012**, *48* (83), 10313-10315, 10.1039/C2CC35543D. DOI: 10.1039/C2CC35543D.
- (35) Béziau, A.; Baudron, S. A.; Rogez, G.; Hosseini, M. W. Assembly, Disassembly, and Reassembly: Conversion of Homometallic Coordination Networks into Mixed Metal–Organic Frameworks. *Inorganic Chemistry* **2015**, *54* (4), 2032-2039. DOI: 10.1021/ic502950k.
- (36) Maeda, H.; Hashimoto, T. Nanoscale Metal Coordination Macrocycles Fabricated by Using "Dimeric" Dipyrrins. *Chemistry A European Journal* **2007**, *13* (28), 7900-7907. DOI: https://doi.org/10.1002/chem.200700444.
- (37) Maeda, H.; Akuta, R.; Bando, Y.; Takaishi, K.; Uchiyama, M.; Muranaka, A.; Tohnai, N.; Seki, S. Formation and Geometrical Control of Polygon-Like Metal-Coordination Assemblies. *Chemistry A European Journal* **2013**, *19* (35), 11676-11685. DOI: <a href="https://doi.org/10.1002/chem.201302028">https://doi.org/10.1002/chem.201302028</a>.

- (38) Zhang, Z.; Dolphin, D. A triple-stranded helicate and mesocate from the same metal and ligand. *Chemical Communications* **2009**, (45), 6931-6933, 10.1039/B913231G. DOI: 10.1039/B913231G.
- (39) Shi, Z.; Han, X.; Hu, W.; Bai, H.; Peng, B.; Ji, L.; Fan, Q.; Li, L.; Huang, W. Bioapplications of small molecule Aza-BODIPY: from rational structural design to in vivo investigations. *Chemical Society Reviews* **2020**, *49* (21), 7533-7567, 10.1039/D0CS00234H. DOI: 10.1039/D0CS00234H.
- (40) Tabone, R.; Feser, D.; Lemma, E. D.; Schepers, U.; Bizzarri, C. Intriguing Heteroleptic ZnII bis(dipyrrinato) Emitters in the Far-Red Region With Large Pseudo-Stokes Shift for Bioimaging. *Frontiers in Chemistry* **2021**, *9*, Original Research. DOI: 10.3389/fchem.2021.754420.
- (41) Higashino, Y.; Erten-Ela, S.; Kubo, Y.  $\pi$ -Expanded dibenzo-BODIPY with near-infrared light absorption: Investigation of photosensitizing properties of NiO-based p-type dye-sensitized solar cells. *Dyes and Pigments* **2019**, *170*, 107613. DOI: https://doi.org/10.1016/j.dyepig.2019.107613.
- (42) Li, G.; Yella, A.; Brown, D. G.; Gorelsky, S. I.; Nazeeruddin, M. K.; Grätzel, M.; Berlinguette, C. P.; Shatruk, M. Near-IR Photoresponse of Ruthenium Dipyrrinate Terpyridine Sensitizers in the Dye-Sensitized Solar Cells. *Inorganic Chemistry* **2014**, *53* (11), 5417-5419. DOI: 10.1021/ic5006538.
- (43) Tsuji, M.; Abuhadba, S.; Chen, A.; Ito, M.; Makhijani, A.; Kuwahara, Y.; Esipova, T.; Mani, T. Red-Colored Circularly Polarized Luminescence from a Benzo-Fused BODIPY-BINOL Complex. *The Journal of Physical Chemistry B* **2023**, *127* (45), 9781-9787. DOI: 10.1021/acs.jpcb.3c05496.
- (44) David, S.; Chateau, D.; Chang, H.-J.; Karlsson, L. H.; Bondar, M. V.; Lopes, C.; Le Guennic, B.; Jacquemin, D.; Berginc, G.; Maury, O.; et al. High-Performance Optical Power Limiting Filters at Telecommunication Wavelengths: When Aza-BODIPY Dyes Bond to Sol–Gel Materials. *The Journal of Physical Chemistry C* **2020**, *124* (44), 24344-24350. DOI: 10.1021/acs.jpcc.0c08006.
- (45) Filatov, M. A.; Lebedev, A. Y.; Mukhin, S. N.; Vinogradov, S. A.; Cheprakov, A. V. pi-Extended Dipyrrins Capable of Highly Fluorogenic Complexation with Metal Ions. *Journal of the American Chemical Society* **2010**, *132* (28), 9552-9554, Article. DOI: 10.1021/ja102852v.
- (46) Hall, J. D.; McLean, T. M.; Smalley, S. J.; Waterland, M. R.; Telfer, S. G. Chromophoric dipyrrin complexes capable of binding to TiO2: Synthesis, structure and spectroscopy. *Dalton Transactions* **2010**, *39* (2), 437-445, 10.1039/B912332F. DOI: 10.1039/B912332F.
- (47) Das, S.; Gupta, I. Triphenylamine substituted dipyrrinato metal complexes: Synthesis, optical and electrochemical studies. *Inorganic Chemistry Communications* **2015**, *60*, 54-60. DOI: https://doi.org/10.1016/j.inoche.2015.07.019.
- (48) Riese, S.; Holzapfel, M.; Schmiedel, A.; Gert, I.; Schmidt, D.; Würthner, F.; Lambert, C. Photoinduced Dynamics of Bisdipyrrinato-palladium(II) and Porphodimethenato-palladium(II) Complexes: Governing Near Infrared Phosphorescence by Structural Restriction. *Inorganic Chemistry* **2018**, *57* (20), 12480-12488. DOI: 10.1021/acs.inorgchem.8b00974.
- (49) Shen, Z.; Röhr, H.; Rurack, K.; Uno, H.; Spieles, M.; Schulz, B.; Reck, G.; Ono, N. Boron–Diindomethene (BDI) Dyes and Their Tetrahydrobicyclo Precursors—en Route to a New Class of Highly Emissive Fluorophores for the Red Spectral Range. *Chemistry A European Journal* **2004**, *10* (19), 4853-4871. DOI: 10.1002/chem.200400173.
- (50) van Stokkum, I. H. M.; Larsen, D. S.; van Grondelle, R. Global and target analysis of time-resolved spectra. *Biochimica et Biophysica Acta (BBA) Bioenergetics* **2004**, *1657* (2), 82-104. DOI: <a href="https://doi.org/10.1016/j.bbabio.2004.04.011">https://doi.org/10.1016/j.bbabio.2004.04.011</a>.
- (51) Kasha, M.; Rawls, H. R.; El-Bayoumi, M. A. The exciton model in molecular spectroscopy. *Pure and Applied Chemistry* **1965**, *11* (3-4), 371-392. DOI: doi:10.1351/pac196511030371 (acccessed 2023-12-29).
- (52) Telfer, S. G.; McLean, T. M.; Waterland, M. R. Exciton coupling in coordination compounds. *Dalton Transactions* **2011**,

- *40* (13), 3097-3108, 10.1039/C0DT01226B. DOI: 10.1039/C0DT01226B.
- (53) Gaussian 16, Revision B.01; Gaussian, Inc.: Wallingford, CT, 2016. (accessed.
- (54) Lu, T.; Chen, F. Multiwfn: A multifunctional wavefunction analyzer. *Journal of Computational Chemistry* **2012**, *33* (5), 580-592. DOI: <a href="https://doi.org/10.1002/jcc.22885">https://doi.org/10.1002/jcc.22885</a>.
- (55) Vinogradov, S. A.; Wilson, D. F. METALLOTETRABENZOPORPHYRINS NEW PHOSPHORESCENT PROBES FOR OXYGEN MEASUREMENTS. *J. Chem. Soc.-Perkin Trans.* 2 **1995**, (1), 103-111, Article. DOI: 10.1039/p29950000103.
- (56) Aartsma, T. J.; Gouterman, M.; Jochum, C.; Kwiram, A. L.; Pepich, B. V.; Williams, L. D. Porphyrins. 43. Triplet sublevel emission of platinum tetrabenzoporphyrin by spectrothermal principal component decomposition. *Journal of the American Chemical Society* **1982**, *104* (23), 6278-6283. DOI: 10.1021/ja00387a021.
- (57) Chow, P.-K.; Cheng, G.; Tong, G. S. M.; Ma, C.; Kwok, W.-M.; Ang, W.-H.; Chung, C. Y.-S.; Yang, C.; Wang, F.; Che, C.-M. Highly luminescent palladium(ii) complexes with sub-millisecond blue to green phosphorescent excited states. Photocatalysis and highly efficient PSF-OLEDs. *Chemical Science* **2016**, *7* (9), 6083-6098, 10.1039/C6SC00462H. DOI: 10.1039/C6SC00462H.
- (58) Kobayashi, T.; Straub, K. D.; Rentzepis, P. M. ENERGY RELAXATION MECHANISM IN Ni(II), Pd(II), Pt(II) and Zn(II) PORPHYRINS. *Photochem. Photobiol.* **1979**, *29* (5), 925-931. DOI: https://doi.org/10.1111/j.1751-1097.1979.tb07793.x.
- (59) Sauvage, J. P.; Collin, J. P.; Chambron, J. C.; Guillerez, S.; Coudret, C.; Balzani, V.; Barigelletti, F.; De Cola, L.; Flamigni, L. Ruthenium(II) and Osmium(II) Bis(terpyridine) Complexes in Covalently-Linked Multicomponent Systems: Synthesis, Electrochemical Behavior, Absorption Spectra, and Photochemical and Photophysical Properties. *Chemical Reviews* **1994**, *94* (4), 993-1019. DOI: 10.1021/cr00028a006.
- (60) Roberts, S. T.; Schlenker, C. W.; Barlier, V.; McAnally, R. E.; Zhang, Y.; Mastron, J. N.; Thompson, M. E.; Bradforth, S. E. Observation of Triplet Exciton Formation in a Platinum-Sensitized Organic Photovoltaic Device. *The Journal of Physical Chemistry Letters* **2011**, *2* (2), 48-54. DOI: 10.1021/jz101554m.

### Insert Table of Contents Graphic and Synopsis



We present synthesis and structures of benzodipyrrin complexes with  $Pd^{2+}$  and  $Pt^{2+}$ . X-ray crystallography showed that both complexes have a zigzag shape with square planar metal coordination. We also explored their electrochemical and optical properties. The  $Pd^{2+}$  complex showed weak fluorescence at 665 nm, while the  $Pt^{2+}$  complex is nonemissive. Transient absorption spectroscopy confirmed short-lived triplet states in both complexes, with no phosphorescence, explained by low-energy ligand-metal charge-transfer triplet state, as revealed by DFT calculations.